Fabrication and characterization of a novel nanoporous nanoaerogel based on gelatin as a biosorbent for removing heavy metal ions

Narjes Nematidil[1] · Shabnam Nezami[1] · Farzad Mirzaie[2] · Edris Ebrahimi[3,4] · Mohammad Sadeghi [ID][5] ·
Nina Farmani[5] · Hossein Sadeghi[6]

Abstract

In this research, we proposed a synthesis of nano-silica aerogel (NSA, $S_1–S_3$) and nano-silica aerogel gelatin (NSA-G, $S_4–S_6$), which were hybrid aerogel by sol–gel method via ambient pressure drying. The aerogels' backbone was modified by montmorillonite (MMT) in NSA and for NSA-G gelatin (G) and MMT were used to stabilize their building block. Also, free hydroxyl groups on their surface were changed to TMS-O and became more hydrophobic aerogels. The porosity results showed that the density of the optimum aerogels (S_2 and S_5) ranged from 0.084 to 0.047 g/cm^3. It was also found that the hydrophobicity of the NSA-G aerogel decreased with increasing the content of gelatin into the silica aerogels. However, these aerogels were fully characterized by FTIR, FESEM, EDS, XRD, BET, and TGA/DTA analysis and they used as the adsorbent of Cu^{2+} and Ni^{2+} ions in aqueous media. The prepared aerogels effectively could remove these heavy metals from the aqueous media and NSA-G absorbent also illustrated a favorable result for adsorption. Also, the recyclability test for four adsorption–desorption of aerogels cycles was examined and they had a good effect even after the fourth cycle.

Graphical Abstract
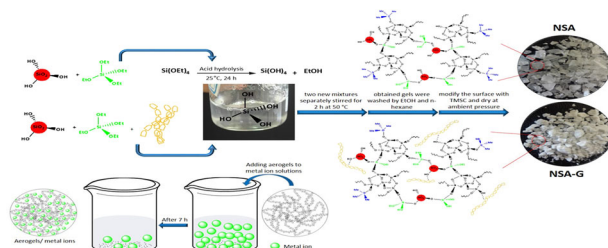
✉ Mohammad Sadeghi
m-sadeghi@iau-arak.ac.ir

1 Young Researchers and Elite club, Arak branch, Islamic Azad University, Arak, Iran

2 Environmental Laboratory, Department of Chemical Engineering, Shiraz University, Shiraz, Iran

3 Department of Chemistry, College of Sciences, Shiraz University, Shiraz 71946-84795, Iran

4 Department of Oncology University of Alberta, Cross Cancer Institute, Edmonton, AB T6G 1Z2, Canada

5 Department of chemistry, Arak branch, Islamic Azad University, Arak, Iran

6 Young Researchers and Elite club, Khorramabad branch, Islamic Azad University, Khorramabad, Iran

Highlights

- The novel NSA and NSA-G as effective adsorbents were successfully prepared.
- The adsorbents exhibited high sorption capacity for adsorbing Cu2^{+} and Ni2^{+} ions.
- TGA/DTG of NSA-G exhibiting more thermal resistance in compare to NSA.
- FESEM result indicating more compact structure for NSA-G with size 46–77 nm.

1 Introduction

This day's heavy metals can cause serious environmental damage in wastewater, which is nonbiodegradable and very toxic, and they affect human health by contaminating water resources [1, 2]. So, removing heavy metals from wastewater is required and several methods have been used, which include membrane filtration [3], chemical precipitation [4], neutralization [5], and adsorption [6]. By comparing these techniques together, the adsorption method has utilized silica aerogels with high porosity, transparency, a high surface area foams [7, 8]. Adsorption method has very effective potential activities to use in several important areas such as carbon dioxide capture [9], aerospace [10], oil-spill absorbencies for replacement in open-cell polymer foams [11], drug delivery [12], and remove heavy metal ions in wastewater [13].

Silica aerogels are also well known as solid fume, that due to low density, high porosity (~98%), large surface area (~1600 m^2/g), low bulk density (~0.03 g/cm^3) easy handling, high efficiency, and recyclability of the adsorbents are widely used [14–16]. The first silica aerogels have been introduced by Samuel Stephens Kistler in 1932 [16], that porous silica structure developed by filling gas instead of liquid in the form of the gel. Also, he has developed silica aerogels via the supercritical fluid drying technique to perform porous solids from the gel. Synthesis of aerogel generally includes two main steps, which are firstly sol–gel process for the synthesis of gel [17] that is a technique for creating solid materials from small molecules and involves an adaptation of monomers into a colloidal solution (sol) that performances to an integrated network (or gel), and secondly is using super critically or ambient pressure for drying gel [18].

The supercritical fluid drying technique is the well-established drying method that has been already used in the silica aerogel industry and generally at this method, fluid is almost at zero surface tension at under supercritical conditions [16, 19, 20]. Thus, this performs ideal conditions to remove water from wet gels while avoiding collapse and shrinkage. However, using high pressures (5–10 MPa) is one of the disadvantages of supercritical drying which requires services of high quality and energy. As an alternative, successful preparation silica aerogel by surface modification under ambient pressure has been reported [21]. Also, the spring back result has

been discovered during ambient pressure drying that it approves acting as a drying control chemical additive which this method can uniform the most of the pore size distribution in silica aerogel [22, 23]. Moreover, solvent exchange and surface modification are other advantages in the ambient pressure drying because it is a favorable method in preparation period which can be done before drying [24]. Despite using water glass is fairly cheap for the preparation of silica aerogels based on tetra ethoxysilane (TEOS) to have the specific surface area, but this is not excellent. For this reason, alcogel granules have been utilized in n-hexane and TEOS as another alternative [25–27].

Bio-aerogel is a novel generation of hybrid aerogels, which has been developed via a cellulose part such as water-soluble gelation, chitosan and polymer and conjugation by non-water-soluble compounds like GO [28] and silicon [29–31]. In this investigation, we prepared six novel NSA and bio-aerogel NSA-G aerogels (S_1–S_6) by sol–gel and drying method and after full characterization of them by using a range of analytical methods, they evaluated and used for the sorption heavy metals Cu^{2+} and Ni^{2+} ions from water in the laboratory situation.

2 Experimental

2.1 Materials

Gelatin type B (average Mw = 190,000–220,000) was extracted from the black tilapia fish wastes in our laboratory [32, 33]. Sodium montmorillonite nanoparticles (MMT) with an average crystalline size 30 nm were purchased from southern clay USA. Tetraethyl ortho-silicate (TEOS), trimethylchlorosilane (TMCS), N,N-dimethylformamide (DMF), and other chemicals (Ethanol, HCl solution, NaOH, n-Hexane) were ACS reagent grade (Sigma-Aldrich). All aqueous solutions were prepared with distilled water.

2.1.1 Preparation of metal ions solution

A stock solution of copper (II) and nickel (II) ions were prepared by dissolving nitrates of them in deionized water. The solutions were further diluted to the required concentrations before use.

Table 1 Synthetic conditions and calculation of the parameters such as adsorption capacity and percentage removal (%R) of the resulting aerogels

Aerogel samples		TEOS (mL)	HCl (M)	Gelatin (%Wt)	MMT (g)	TMCS/n-Hexane	Adsorption capacity (mg/g)		%R	
							Cu^{2+}	Ni^{2+}	Cu^{2+}	Ni^{2+}
	S1	2	0.1	0	0.7	1/6	240.7	210.9	65.4	60.5
NSA	S2	4	0.2	0	1.4	1/3	330.9	311.8	82.1	77.3
	S3	6	0.3	0	2.1	1/2	301.5	297.3	59.4	54.8
	S4	2	0.1	10	0.7	1/6	254.8	238.4	68.2	63.7
NSA-G	S5	4	0.2	20	1.4	1/3	368.5	338.7	90.4	84.2
	S6	6	0.3	30	2.1	1/2	310.7	305.2	71.4	66.4

2.2 Synthesis of NSA and NSA-G adsorbents by drying at ambient pressure

Pristine NSA and NSA-G aerogels (S$_1$–S$_6$) were prepared through hydrolysis and poly-condensation using TEOS precursors via a sol–gel polymerization process. At first, to synthesize adsorbents NSA (S$_1$–S$_3$) and NSA-G (S$_4$–S$_6$) two solutions A and B were prepared. The solution A was prepared by a mixture of TEOS, ethanol, dimethyl formamide, and distilled water, with a mole ratio of 1: 8: 0.5: 2, and a few drops of hydrochloric acid was added to hydrolyze of TEOS and stirred at room temperature for 24 h. The solution of B containing a mixture of alkali (pH = 8) MMT and TEOS with various ratio was prepared and stirred for 2 h at 50 °C. NSAs were synthesized by adding solution B to solution A, but for NSA-G adsorbents, the solution of B with various amounts of the preprepared gelatin was added to solution A according to Table 1, and two new mixtures separately stirred for 1 h at 50 °C. The solutions were converted to gel-form and the obtained gels were washed by EtOH and n-hexane for several times to remove the residual solvents and non-reactant materials. Wet gels were placed in various ratio TMSC/n-Hexane solution for 24 h at 30 °C water baths to modify the surface with TMSC (hydrophobic-up). Then the gels were removed and washed with hexane and kept at 60 °C for 10 and 24 h at room temperature to dry with a slight contraction.

2.3 Adsorption study

Batch adsorption experiments were conducted by adding the different amounts of the NSA and NSA-G aerogels (S$_1$–S$_6$) into 200 mL of copper nitrate and nickel nitrate solution with the different pH values and then shaking the mixture in a thermostatic shaker bath at a certain temperature (288–308) for 7 h. The pH value of the copper nitrate solution was adjusted by a diluted nitric acid or sodium hydroxide solution and was measured by a pH-meter. Then, the copper and nickel concentrations of solutions before and after adsorption were determined by atomic absorption spectroscopy (AAS). It should be noted that this procedure

was repeated three times for each metal, and the average percentage values of extracted metal ion were calculated. The amount of metal ion adsorbed was calculated by Eqs. 1 and 2 at equilibrium (q_e (mg/g), and the percentage of metal ion removal per unit mass of the biosorbent, R) [34].

$$q_e = \frac{(C_\circ - C_e)}{w} \times V, \tag{1}$$

$$\%R = \frac{(C_\circ - C_e)}{C_\circ} \times 100. \tag{2}$$

2.4 Desorption and reusability

Desorption of the heavy metal ions was performed by the optimum aerogels (S$_2$ and S$_5$) at adsorption equilibrium, with Cu^{2+} and Ni^{2+} ions were placed in the 200 mL of various solutions of 0.05 M HCl as the eluting agents for 6 h, at ambient temperature, and the mixtures were shaken with the speed of 150 rpm. Then, the mixtures were centrifuged at 6000 rpm for 15 min and the concentration of the eluted metal ions was measured according to Eq. 3 where C_d is the metal ions concentration in the desorption solutions (mg/l), V_d is the volume of the desorption solution in a liter, respectively, and V is the volume of the solution in a liter [35].

$$\%D = \frac{C_d V_d}{(C_0 - C_e)V} \times 100. \tag{3}$$

2.5 Characterization methods

Infrared (IR) spectra were recorded by Fourier transform infrared spectroscopy spectrometer (FTIR, SHIMADZU, 8400S model) in the wavenumber range of 400–4000 cm^{-1}. X-ray diffraction (XRD) pattern was obtained in the 2θ range of 2–30° with wavelength λ = 1.54 A to observe modifications on crystalline of optimum aerogels (S$_2$ and S$_5$) backbone based on the pattern and appearance new peak, by X-ray diffractometer (Bruker AXS-D8 Advance model). FESEM (TE-SCAN) analysis was performed to
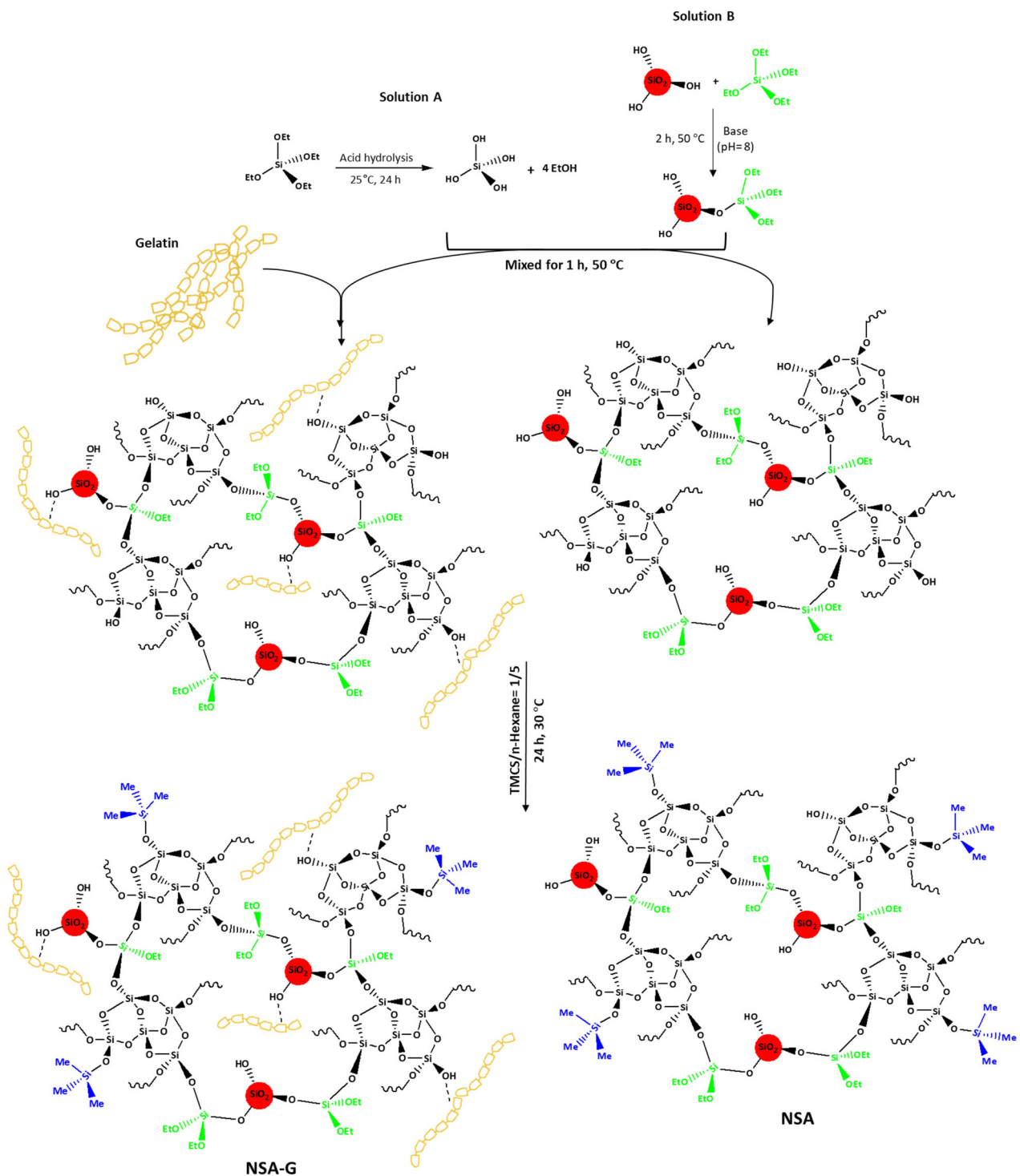
Scheme 1 The schematic pattern for the preparation of NSA (S_1–S_3) and the NSA-G (S_4–S_6)

find of morphology and shape modified nano-silica inside the NSA (S_2) and NSA-G (S_5). Thermal analyses (TGA/DTG) of NSA (S_2) in comparing to NSA-G (S_5) was performed by using the Netzsch-TGA 209 F1 analyzer under a temperature range of 20–900 °C with the heating rate of 10 °C/min under the nitrogen flow rate of 10 mL/min. The

specific surface area SBET (Brunauer–Emmett–Teller), pore volumes, and average pore size of both obtained materials (S_2 and S_5) were analyzed by nitrogen adsorption/desorption isotherms and BJH (Barrett–Joyner–Halenda) pore diameters methods using a model NOVA 3200e automated gas sorption system. Hydrophobicity of the

optimum aerogels (S$_2$ and S$_5$) was analyzed by measuring the contact angle (θ) of the water droplet with the sample surface by using the CA-500 Optical microscope model. For measurement of the concentration of the metal ions, the atomic absorption spectrometer (AAS-Shimadzu model AA-680) was also applied.

The porosity of the optimum aerogels (S$_2$ and S$_5$) was calculated using the density of the NSA (S$_2$) and NSA-G (S$_5$) aerogels (ρ_{Gel}) and density of the skeleton (ρ_{TEOS}) after enough drying samples according to Eq. 4. The bulk density of the aerogel samples (S$_2$ and S$_5$) was calculated by measuring its mass to volume ratio with help of bulk density meter. For all of the experiments, data were expressed as means values ± standard deviation (SD) of three parallel measurements [18].

$$p\,(\%) = 100 \times (1 - \rho_{Gel}/\rho_{TEOS}) \tag{4}$$

In the above equations, ρ_{Gel} is the bulk density of aerogel and ρ_{TEOS} is the skeleton density of the silica aerogels. Generally, the value of ρ_{TEOS} is 940 kg/m^3 [36].

3 Results and discussion

3.1 Proposed mechanism for the synthesis of NSA and NSA-G aerogels

For the synthesis silica-based hydrophobic aerogels (S$_1$–S$_6$) two solutions of A and B were prepared. Solution A contained a mixture of TEOS, ethanol, DMF, distilled water, and a few drops of hydrochloric acid to hydrolyze TEOS for forming silica chains. In solution B, alkaline MMT (pH = 8) and TEOS were mixed to modify MMT surface with TEOS. Then, by mixing solutions A and B, NSA was made. For the synthesis of NSA-G (S$_4$–S$_6$), gelatin was added to solution B, and gelatin chains were connected to the active site of OH on the silicone. Followed by adding current solution B to solution A, the active groups of OH on the silica chains coupled via gelatin chains and MMT. Finally, to hydrophobic the surface, the remaining OH groups on the silica chains converted to O–Si(Me)$_3$ by adding TMSC as shown in the following schematic Scheme 1.

3.2 Characterization of NSA (S$_2$) and NSA-G (S$_5$) aerogels

3.2.1 FTIR spectrum

The FTIR spectrum of the starting materials and prepared aerogels (S$_2$ and S$_5$) are shown in Fig. 1. As can be seen from the Fig. 1A, the appearance peak in 1646 cm^{-1} related to the stretching vibration of the carboxamide group and a fairly wide peak at 3150–3436 cm^{-1} was also relative to the stretching vibration of the NH$_2$ group in the gelatin's
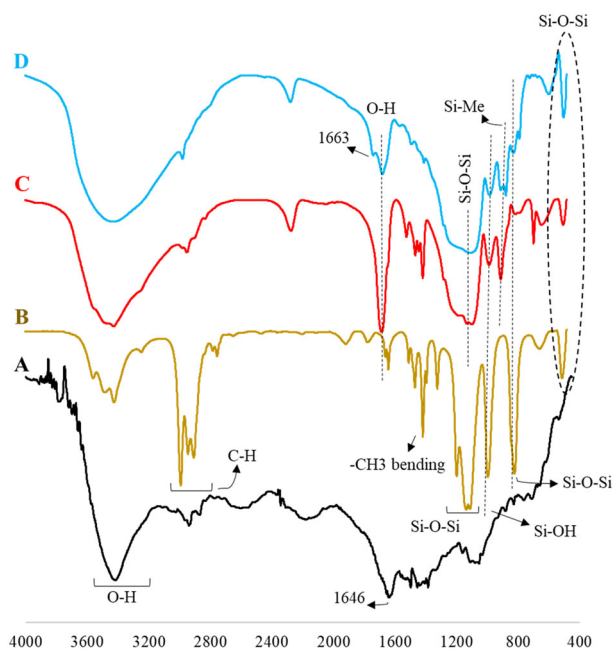

Fig. 1 The FTIR spectrum of gelatin (A), TEOS (B), NSA (S$_2$) (C), and NSA-G (S$_5$) (D)

building. The strong peaks were shown in all three spectra B, C, and D in the 476–489 cm^{-1} region could be attributed to Si–O–Si bending vibration. Moreover, the appearance peaks in the regions 789–799 and 1064–1081 cm^{-1} were attributed to the symmetric and asymmetric stretching vibration of Si–O–Si, respectively. Also, the spectrum showed a peak in the 949–967 cm^{-1} for the Si–O stretching vibration and two peaks at 1660–1660 and 3407–3423 cm^{-1} for the stretching vibration of O–H and a peak in the 2893–2990 cm^{-1} for the stretching vibration of C–H, respectively. A peak in the 848–883 cm^{-1} range was found in the NSA (S$_2$) and NSA-G (S$_5$) (Fig. 1C, D) spectra corresponding to the stretching vibration of Si–C. This peak was not seen in TEOS and it confirmed the presence of Si–CH$_3$ groups in surface aerogel by TMSC.

3.2.2 EDS and FESEM techniques

The elemental analysis, size and morphology of NSA (S$_2$) and NSA-G (S$_5$) surfaces before and after Cu^{2+} and Ni^{2+} ions sorption were shown in Fig. 2. As shown in Fig. 2A there were no significant differences in the 2 μm and 200 nm by comparing two forms of NSA-G (S$_5$) and NSA (S$_2$). NSA-G (S$_5$) showed a more compact structure, which was characterized by smaller particles, heterogeneous agglomerates, and density of spherical nanoparticles with variable sizes ranges from 46 to 77 nm while the size of nanoparticles in the NSA (S$_2$) was in the range of 59–103 nm. The composition of the prepared materials was assessed
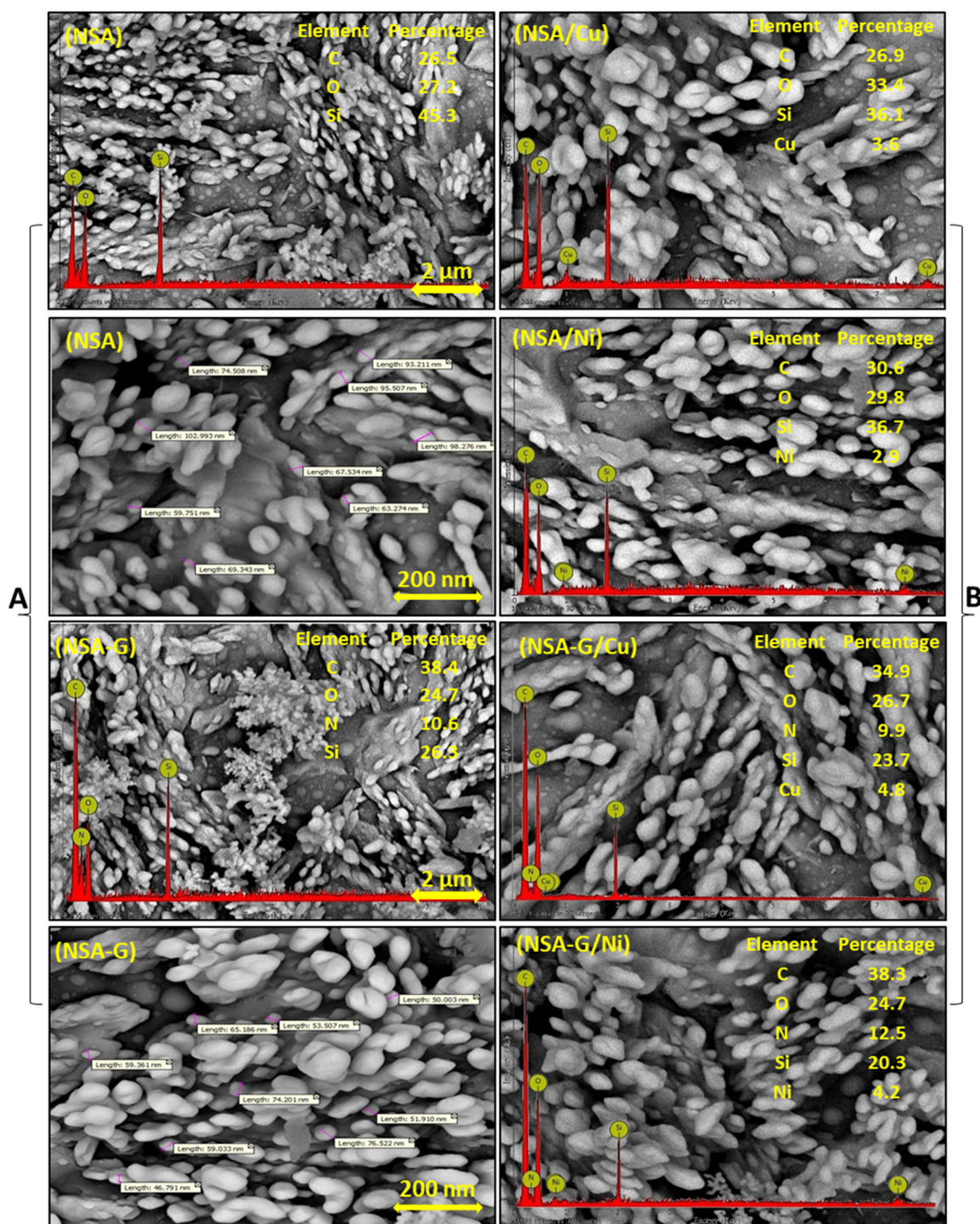
Fig. 2 The FESEM images and EDX spectra of the NSA (S_2) and the NSA-G (S_5) before (in the 2-scale of 2 μm and 200 nm) (**A**) and after (in the scale of 1 μm) Cu^{2+} and Ni^{2+} ions sorption (**B**)

using energy dispersive spectroscopy (EDS). According to Fig. 2A, the percentage of elemental composition estimated from the EDS analysis were C (26.5), O (27.2), and Si (45.3) as main components of the NSA (S_2) aerogel and the main elements of the NSA-G (S_5) were C (38.4), O (24.7), N (10.6), and Si (26.3), respectively. The presence of

nitrogen element in the EDS of NSA-G (S_5) aerogel specified the significant presence of gelatin molecules inside of the polymer matrix with no other contaminants. The FESEM images and EDX of the NSA (S_2) and the NSA-G (S_5) after Cu^{2+} and Ni^{2+} ions sorption were investigated and the results shown in Fig. 2B. By comparing FESEM images

of prepared adsorbents before and after adsorption of the metal ions obviously changed the surface morphology of the prepared materials (S_2 and S_5) during the sorption process on both adsorbents. Furthermore, the EDS results of the samples were a clear indication for the successful Cu^{2+} and Ni^{2+} ions loading on the surface of both adsorbents [37, 38].

3.2.3 X-ray diffraction (XRD)

The XRD spectra of the optimum aerogels (S_2 and S_5) were taken in the range of $2\theta = 0$–$30°$ and were shown in the Fig. 3A–D. It can be seen from the Fig. 3A, B, the MMT nanoparticles revealed a peak at $2\theta = 21.2°$, although gelatin showed any peak in this range. After adding MMT nanoparticles to the polymeric network, due to the dispersion of MMT nanoparticles, the peak diffusion of MMT nanoparticles in the nano-aerogels network appeared at a lower angle with less intensity. According to the NSA (S_2) XRD spectrum shape, it showed a sharpness peak at $2\theta = 19.1°$ (Fig. 3C), whereas the NSA-G (S_5) XRD exhibited a polygonal region at $2\theta = 19.9°$. The extension of the peak confirmed the addition of gelatin to the aerogel network and prevented the agglomeration of the MMT nanoparticles (Fig. 3D). Also, the average size of MMT nanoparticles trapped in the nanocomposite network was calculated 52 and 79 nm by the Debye-Scherrer method for NSA-G (S_5) and NSA (S_2), respectively.

3.2.4 Study of the specific surface area and the distribution of cavities in aerogels (BET and BJH)

For providing more accurate evidence on the formation of the gelatin-based aerogels from aerogels, the BET and BJH
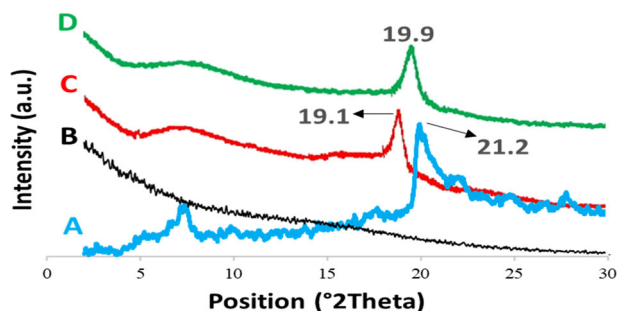
techniques were applied and the obtained results such as the specific surface area, cavity volume, and the average diameter of the cavities were tabulated in Table 2. The results showed that the volume of the NSA (S_2) cavities was larger than the NSA-G (S_5) and the calculated specific surface area (SBET) for the NSA-G (S_5) was greater than the NSA (S_2), which indicated the presence of the aggregated gelatin and more cross-linking in the NSA-G (S_5) network. Figure 4A also showed the type of NSA (S_2) and NSA-G (S_5) isotherm belong to the type IV and hysteresis ring belonging to type C. This similarity indicated the aerogels type in meso form with cone-shaped holes. Figure 4B showed the distribution of the pore size of the aerogels that the NSA (S_2) had a relatively narrow curve and most of the pores were the meso form, while the NSA-G (S_5) had a fairly wide pore size and fewer alignments between pores. On the other hand, as shown in Table 2, the porosity results indicated that the addition of the gelatin into the silica aerogels influenced their properties and it caused that the average porosity of the aerogels linearly increased from 91 to 95%.
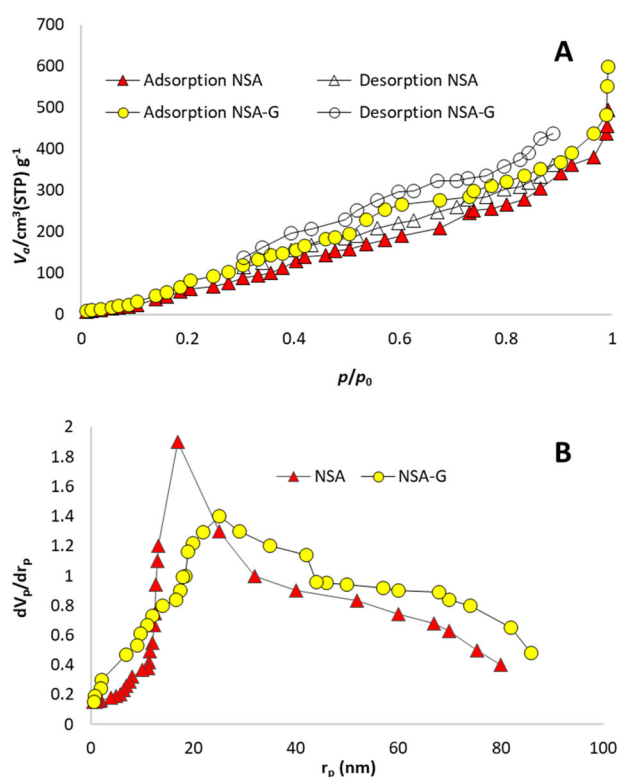

Fig. 4 Adsorption and desorption isotherms (**A**) and BJH charts (**B**) of nano-aerogels (S_2 and S_5)

Fig. 3 XRD spectrum of the MMT (**A**), gelatin (**B**), NSA (S_2) (**C**), and NSA-G (S_5) (**D**)

Table 2 Bulk density, porosity, specific surface area pore volume, and average diameters cavities of nano-aerogels (S_2 and S_5)

Samples	Bulk density (g/cm^3)	Porosity (%)	Specific surface area (m^2/g)	Pore volume (cm^3/g)	Average pore size (nm)
NSA (S_2)	0.084 (±0.002)	91 (±0.09)	264	1.2	16.6
NSA-G (S_5)	0.047 (±0.002)	95 (±0.09)	332	0.94	24.3

3.2.5 Angle contact measurement

Figure 5 showed the contact angle of the synthesized aerogels (S_2 and S_5) with a drop of water and the contact angle for both adsorbents was greater than 90°, which indicated the hydrophobicity of the aerogels. Decreasing the angle of contact in the NSA-G (S_5) showed that the process of adding gelatin caused a slight decrease in the hydrophobicity (see Fig. 5B). Figure 5C showed the (S_5), due to the high porosity, had a lower density than water and were placed on the water.

3.2.6 TGA and DTG thermal analysis

TGA/DTG analysis was used to study the thermal stability of the prepared aerogels (S_2 and S_5) that thermal analysis was checked by increasing the temperature from 25 to 900 °C as shown in Fig. 6. According to the thermogram, when the temperature increased to 150 °C, the thermogram showed a slight percentage of the loose weight of the NSA (S_2) and NSA-G (S_5), because of the evaporation of water from the pore and inner layers of aerogels. However, in this range of temperature, it is clearly revealed that NSA-G (S_5) suffers a greater weight loss as compared to the NSA(S_2) and this probably indicates the further loss of moisture from the NSA-G (S_5) network. By increasing the temperature, NSA (S_2) showed two-weight-loss about 3% and 5% at 300 and 380 °C, respectively which could be changing the conformation of aerogel. However, the NSA-G (S_5) during this temperature did not have a big change in its chromatogram, and this result can be due to the presence of gelatin in the structure of NSA-G (S_5) made significant stability. With the further increase in temperature up to 450 °C, no significant difference was found in the thermal resistance of the two adsorbents and both aerogels had a similar trend of total weight loss. In continue, after 683 °C, the weight loss of NSA-G (S_5) was more as compared to the NSA (S_2) sample that this can be probably due to the presence of gelatin in the polymer matrix.

3.3 Absorption studies of copper and nickel metal ions on NSA (S_2) and NSA-G (S_5)

3.3.1 The effect of contact time

To determine the contact time effect on the adsorption capacity and the removal percent efficiency of Cu^{2+} and Ni^{2+}, adsorbents were investigated at 298 K for 1–16 h. As shown in Fig. 7A, the adsorption capacity and removal percentage for both adsorbents improved with increasing reaction time to reach the equilibrium after 5 h for the NSA-
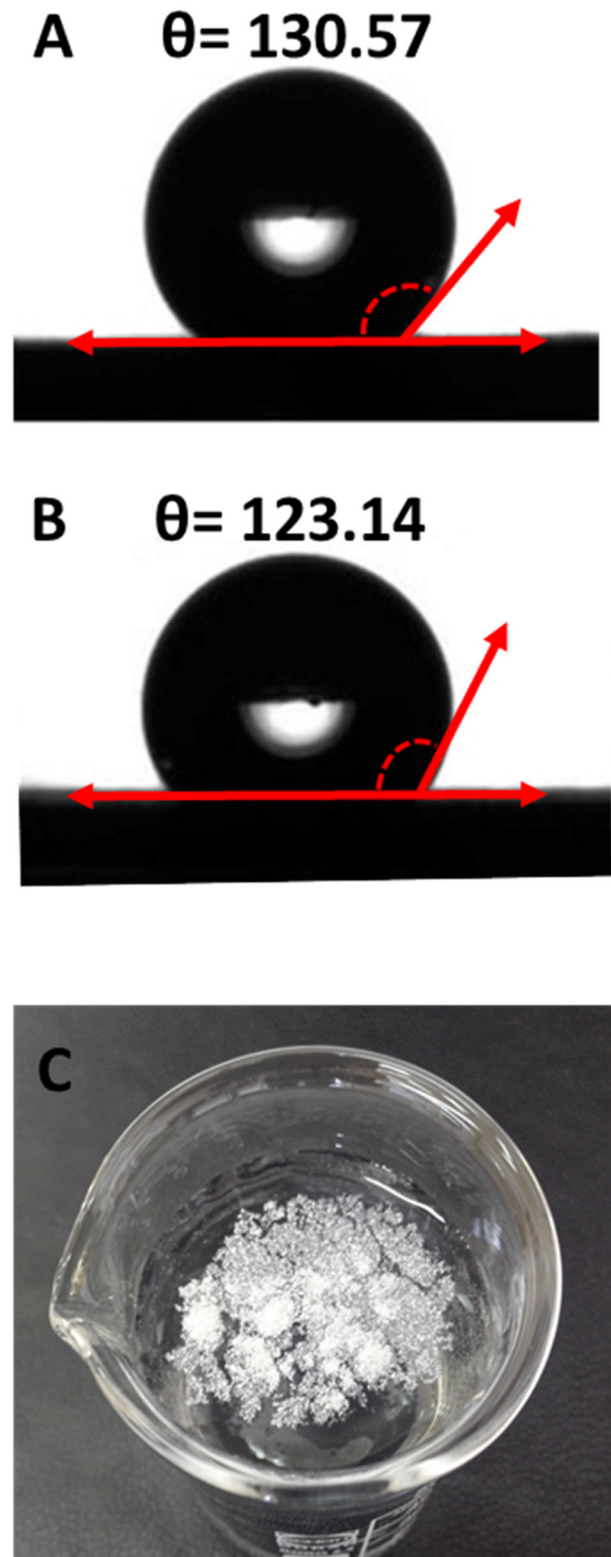
Fig. 5 Angle contact with drop water for NSA (S_2) (**A**), NSA-G (S_5) (**B**), and nanoaerogel (S_5) float on the surface of the water (**C**)

G (S_5) and 7 h for the NSA (S_2) and after these times, absorption remained almost constant. This rapid absorption

in the early stages of the process can be due to the abundance and availability of active groups on the surface of the adsorbents [39], where the gradual occupancy of these active sites during the lapse of time, the metal ions sorption becomes less efficient [39, 40].

Moreover, the results revealed that the removal efficiency of NSA-G (S_5) for both metal ions was higher than the NSA (S_2). These findings confirmed the modification of NSA (S_2) aerogel with gelatin to formed NSA-G (S_5) caused to have more porosity and consequently the further
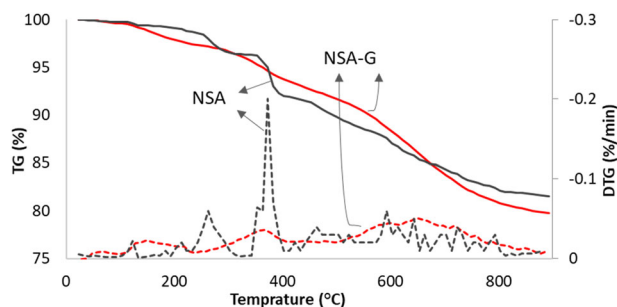

Fig. 6 TGA and DTG spectra of the nano-aerogels (S_2 and S_5)

adsorption capacity at less time. Table 3 indicates the comparison of the maximum adsorption capacity of the different adsorbents for Cu^{2+} and Ni^{2+} ions. It is revealed that both prepared aerogels (S_2 and S_5) had greater potential adsorption than the other reported silica-based adsorbent for the sorption of these metal ions.

3.3.2 The pH effects

pH effect was examined for 0.1 g of NSA and NSA-G (S_2 and S_5) separately in 200 mL solution of Cu^{2+} and Ni^{2+} (200 ppm) at pH 3.0–8.0 for 7 h. As shown in Fig. 7B, changes in the pH solution caused significant variation in adsorption capacity. The maximum adsorption of Cu^{2+} and Ni^{2+} ions for NSA and NSA-G (S_2 and S_5) were at pH 5.5 and 6.5, respectively. It was also noteworthy that in this study, pH > 8 was not used, because, under these conditions, the reaction between Cu^{2+} and Ni^{2+} ions and OH^- ions happened and produced various species precipitate such as MOH^+ and $M(OH)_2$. Also, only small amounts of ions were trapped at pH < 3, which was probably due to the protonation of OH groups within adsorbent networks in

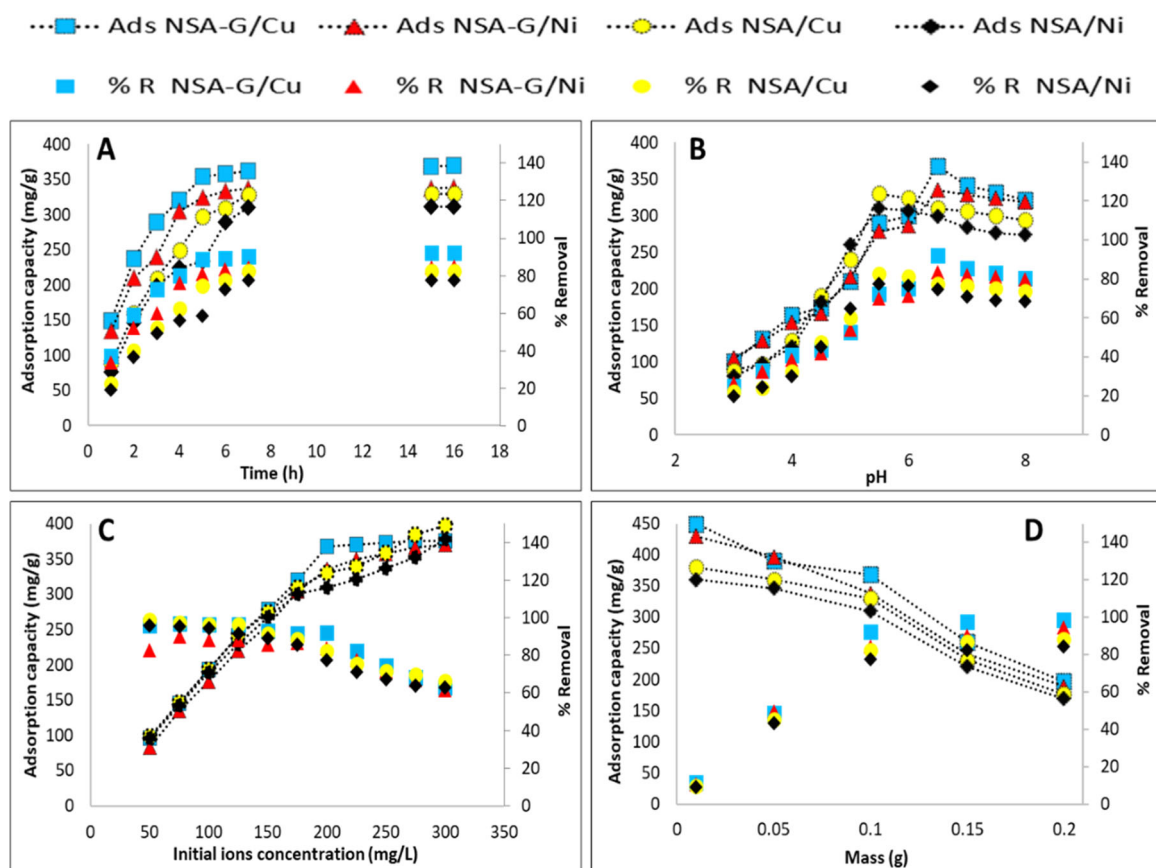Fig. 7 Effect of contact time (**A**), pH solution (**B**), initial ions concentration (**C**), and mass of adsorbents (S_2 and S_5) (**D**) on the adsorption capacity and removal percentage

Table 3 Comparison of sorption capacity of the prepared NSA and NSA-G (S_2 and S_5) with some recently reported bioadsorbent

| Sorbent	Adsorption capacity (mg/g)		Reference
	Cu^{2+}	Ni^{2+}	
ATP/P(AA-co-AM)	30.35	–	[45]
CTA/Silica	–	64.18	[46]
P-PAN	78.06	–	[47]
PolyAN/organobentonite composite	77.430	–	[48]
Modified silica aerogel	90.1	–	[49]
PLCD	98	67	[50]
CTS/PNN	29	20	[51]
NSA (S_2)	330.9	311.8	This work
	$R = 82.1\%$	$R = 77.3\%$	
NSA-G (S_5)	368.5	338.7	This work
	$R = 90.4\%$	$R = 84.2\%$	

highly acidic conditions. These results are in good agreement with the results that have been reported by other researchers [41].

3.3.3 The effect of the concentration of the initial metal ion

The initial concentration of Cu^{2+} and Ni^{2+} ions in the range of 50–300 mg/L at 298 K was investigated. As shown in Fig. 7C, upon increasing the initial ion concentrations from 50 to 300 mg per 1 liter, the optimum adsorption capacity of the ions increased. At higher concentrations for both adsorbents, the sorption of copper ions remained almost constant due to the occupation or saturation of active sites on the adsorbent surface. However, by increasing the initial concentration of metal ions, the adsorption rate of these ions decreased, but the adsorption capability increased. By increasing the initial concentration of metal ions, the number of rival ions improved to react with active groups of the adsorbent surface and adsorbent active sites were saturated. In other words, the adsorption capacity was enhanced with increasing concentration of metal ions in the solution. Enhancing the concentration of metal ions led to an increase in the number of interactions between metal ions and adsorbents, which, in turn, accelerated the adsorption process [42].

3.3.4 Adsorbents effect

The amount of adsorbents in the range of 0.01–0.2 g was investigated and their results were shown in Fig. 7D. As can be seen in the figure, increasing the amount of aerogels (S_2 and S_5) led to an increase in the removal percent. On the
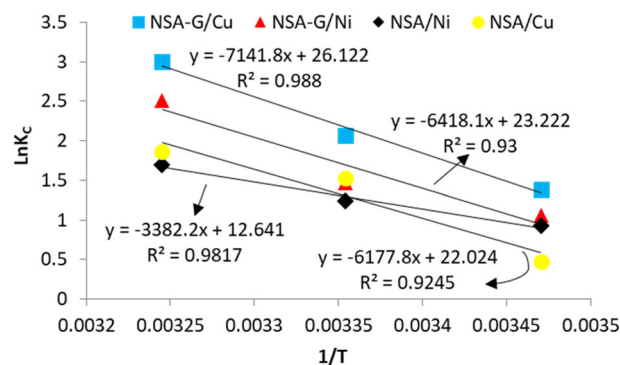
Fig. 8 The plot of Ln K_d against 1/T for NSA and NSA-G (S_2 and S_5)

other hand, increasing in the amount of aerogels (S_2 and S_5) caused to decrease in adsorption capacity, but in general, the adsorption rate was enhanced by increasing adsorbent content due to the enhancement in the number of active sites. Improvement in adsorption capacity happened by increasing adsorbent because the accumulation of these particles led to a decrease in total adsorbent content [43].

3.3.5 Temperature and thermodynamics effect study

In these series of experiments, changing the removal of ions was studied at 288–308 K by using NSA and NSA-G aerogels (S_2 and S_5) and the results were shown in Fig. 8. The data revealed that the removal rate was enhanced with increasing temperature for both aerogels and indicated thermosensitive of the process of adsorption of Cu^{2+} and Ni^{2+} ions on the aerogels. To this purpose, thermodynamic parameters such as changing in the Gibbs free energy ($\Delta G°$, KJ/mol), enthalpy ($\Delta H°$, KJ/mol) and entropy ($\Delta S°$, J/mol K) of the system were calculated based on the Eqs. 5–7 and are listed in Table 4. In these equations, R is gas constant (8.314 J/mol K), T temperature in Kelvin (K), C_{Re} equilibrium concentration metal ion in the adsorbent (mg/L), and C_{Se} equilibrium concentration of metal ions in solution (mg/L).

$$\Delta G° = -RT \ln K_c, \tag{5}$$

$$K_c = \frac{C_{Re}}{C_{Se}}, \tag{6}$$

$$\ln K_c = \frac{\Delta H°}{RT} + \frac{\Delta S°}{R}. \tag{7}$$

As can be seen in Table 4, the highest removal of ions was obtained at 308 K. These results showed that at the highest temperature, the adsorption of Cu^{2+} and Ni^{2+} ions were the highest in both adsorbents. In addition, the positive change values in enthalpy and entropy, and in total, the
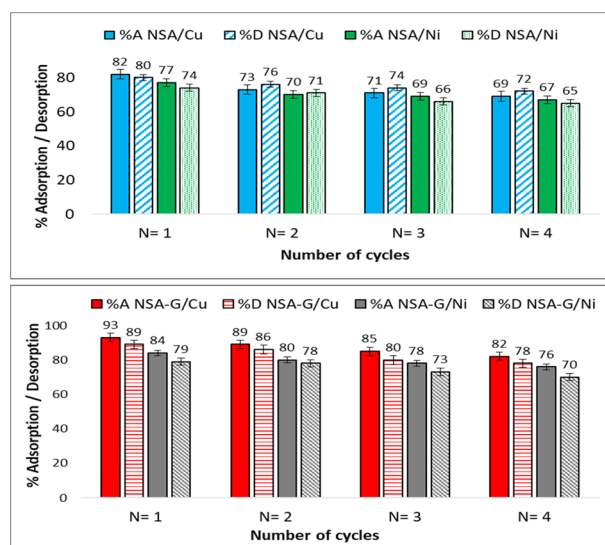
Table 4 Thermodynamic parameters for adsorption of Cu^{2+} and Ni^{2+} ions on aerogels (S_2 and S_5) at three temperatures

Aerogels/M^{2+}	Thermodynamic parameters	Temperature (K)		
		288	298	308
NSA(S_2)/Cu^{2+}	Kc	2.603	4.633	6.407
	ΔG (kJ mol^{-1})	−2.292	−3.801	−4.758
	ΔH (kJ mol^{-1})	33.331		
	ΔS (kJ mol^{-1} K^{-1})	123.928		
NSA(S_2)/Ni^{2+}	Kc	2.539	3.444	5.451
	ΔG (kJ mol^{-1})	−2.233	−3.066	−4.345
	ΔH (kJ mol^{-1})	28.119		
	ΔS (kJ mol^{-1} K^{-1})	105.097		
NSA-G(S_5)/Cu^{2+}	Kc	4.000	7.889	20.052
	ΔG (kJ mol^{-1})	−3.321	−5.119	−7.682
	ΔH (kJ mol^{-1})	59.377		
	ΔS (kJ mol^{-1} K^{-1})	217.178		
NSA-G(S_5)/Ni^{2+}	Kc	2.883	4.334	12.332
	ΔG (kJ mol^{-1})	−2.537	−3.634	−6.436
	ΔH (kJ mol^{-1})	53.360		
	ΔS (kJ mol^{-1} K^{-1})	193.067		

Fig. 9 Recyclability of NSA and NSA-G (S_2 and S_5) for Cu^{2+} and Ni^{2+} metal ions

negative values of Gibbs free energy confirm that the process of adsorbing was spontaneously in nature [44]. Comparing the negative values of NSA-G (S_5) Gibbs free energy, it could be concluded that the process of adsorbing metal ions on NSA-G (S_5) was more favorable than NSA (S_2), so that the maximum adsorption capacity balance (q_e (mg/g)) was observed for Cu^{2+} and Ni^{2+} ions in the presence of NSA-G (S_5) was 381.68, 370.36 and for NSA (S_2) was 346.24, 338.73, respectively.

3.3.6 Investigating the recyclability of adsorbents and their activity in the absorption and desorption of metal ions

The recovery of adsorbents was studied by adsorption and desorption of metal ions from the levels of the aerogels (S_2 and S_5). Initially, the aerogels were washed with deionized water, 200 mL of 0.05 M HCl solution for 6 h and then deionized water, successively. The results of the four adsorption–desorption steps in the presence of metal ions were shown in Fig. 9. As could be seen in the figure, with relocation from the first cycle to the third cycle, the adsorption of Cu^{2+} and Ni^{2+} ions were declined from 82 to 71% and 77 to 69% for NSA (S_2) and 93–85%, and 84–78% for NSA-G (S_5) aerogels, respectively. In addition, the average adsorption percentage Cu^{2+} and Ni^{2+} ions after the fourth cycle for NSA (S_2) and NSA-G (S_5) were 69%, 67%, and 82%, 76%, respectively and these results were exactly satisfactory. In fact, this slight decrease in adsorption showed that active sites on aerogels had not been

completely recycled at the end of each period. In overall, results showed that after four periods of adsorption and desorption of ions, both aerogels had considerable potential for the adsorption of metal ions.

4 Conclusion

Our purpose in this investigation was the synthesis of NSA and NSA-G aerogels (S_2 and S_5) as novel hydrophobic adsorbents that they could able to adsorb soluble ions without absorbing water. These aerogels surface were modified by TMS-O which appeared in the range 848–883 cm^{-1} in the IR spectrum. Investigation of surface morphology of aerogels showed that NSA-G (S_5) illustrated a better structural significance than NSA (S_2), which is included a more compact structure, composed by smaller particles, heterogeneous, and dense agglomerates of spherical nanoparticles with various sizes ranging from 46 to 77 nm, whereas the size of the nanoparticles in the NSA (S_2) was in the range of 59–103 nm. Also, TGA of aerogels exhibited a high thermal resistance and decomposition for the NSA-G (S_5) than NSA (S_2) due to the presence of gelatin. In addition, the XRD spectra of the synthesized aerogels (S_2 and S_5) showed a sharp main peaks at $2\theta =$ 19.1° and 19.9° for the NSA (S_2) and NSA-G (S_5), respectively. Also, the XRD results confirmed the addition of gelatin to the aerogel network prevented the agglomeration of the MMT nanoparticles. According to the results of the BET technique, the NSA (S_2) had a larger volume of cavities than the NSA-G (S_5), but the NSA-G (S_5) had a greater specific area than the NSA (S_2). The contact angle for both adsorbents was greater than 90°, that this indicating

the hydrophobic property of the aerogels and the NSA (S_2) showed a greater contact angle than NSA-G (S_5) because of a slight decrease in the hydrophobicity. On the basis of the porosity of 91–95%, the removal rate for NSA and NSA-G (S_2 and S_5) increased by increasing temperature for both aerogels, which shows that the process of adsorption of Cu^{2+} and Ni^{2+} ions on the aerogels was thermosensitive. Negative values in Gibbs free energy indicated spontaneously in adsorption nature and the adsorption of metal ions process on NSA-G (S_5) was more favorable than NSA (S_2). The results of recyclability after four absorption–desorption of aerogels had considerable potential for adsorption of metal ions. Also, drying and recycling of these adsorbents were fast and less costly due to the lack of water absorption.

Compliance with ethical standards

Conflict of interest The authors declare that they have no conflict of interest.

Publisher's note Springer Nature remains neutral with regard to jurisdictional claims in published maps and institutional affiliations.

References

1. Tian Z, Zhang L, Shi G, Sang X, Ni C (2018) The synthesis of modified alginate flocculants and their properties for removing heavy metal ions of wastewater. J Appl Polym Sci 135:46577
2. Nemati Dil N, Sadeghi M (2018) Free radical synthesis of nano-silver/gelatin-poly (acrylic acid) nanocomposite hydrogels employed for antibacterial activity and removal of Cu(II) me ions. J Hazard Mater 351:38–53
3. Efome JE, Rana D, Matsuura T, Lan CQ (2018) Experiment and modeling for flux and permeate concentration of heavy metal ion in adsorptive membrane filtration using a metal-organic framework incorporated nanofibrous membrane. Chem Eng J 352:737–744
4. Fakhre NA, Ibrahim BM (2018) The use of new chemically modified cellulose for heavy metal ion adsorption. J Hazard Mater 343:324–331
5. Baiya C, Nannuan L, Tassanapukdee Y, Chailapakul O, Songsrirote K (2019) The synthesis of carboxymethyl cellulose-based hydrogel from sugarcane bagasse using microwave-assisted irradiation for selective adsorption of copper (II) ions. Environ Prog Sustain Energy 38:S157–S165
6. Nguyen TC, Loganathan P, Nguyen TV, Kandasamy J, Naidu R, Vigneswaran S (2018) Adsorptive removal of five heavy metals from water using blast furnace slag and fly ash. Environ Sci Pollut R 25:20430–20438
7. Hasegawa G, Shimizu T, Kanamori K, Maeno A, Kaji H, Nakanishi K (2017) Highly flexible hybrid polymer aerogels and xerogels based on resorcinol-formaldehyde with enhanced elastic stiffness and recoverability: Insights into the origin of their mechanical properties. Chem Mater 29:2122–2134
8. Meador MAB, Alemán CR, Hanson K, Ramirez N, Vivod SL, Wilmoth N, McCorkle L (2015) Polyimide aerogels with amide

cross-links: a low cost alternative for mechanically strong polymer aerogels. ACS Appl Mater Interfaces 7:1240–1249
9. Lin YF, Syu CR, Huang KW, Lin KYA (2019) Synthesis of Silica Aerogel Membranes using Low-Cost Silicate Precursors for Carbon Dioxide Capture. Chem Phys Lett 726:13–17
10. Meador MA, Miranda F, Van Keuls F (2016) Aerogel-based antennas for aerospace and terrestrial applications. In Google Patents. https://patents.google.com/patent/US10446920B1/en
11. Mi HY, Jing X, Huang HX, Peng XF, Turng LS (2018) Superhydrophobic graphene/cellulose/silica aerogel with hierarchical structure as superabsorbers for high efficiency selective oil absorption and recovery. Ind Eng Chem Res 57:1745–1755
12. Follmann HD, Oliveira ON, Lazarin-Bidóia D, Nakamura CV, Huang X, Asefa T, Silva R (2018) Multifunctional hybrid aerogels: hyperbranched polymer-trapped mesoporous silica nanoparticles for sustained and prolonged drug release. Nanoscale 10:1704–1715
13. Kabiri S, Tran DN, Azari S, Losic D (2015) Graphene-diatom silica aerogels for efficient removal of mercury ions from water. ACS Appl Mater Interfaces 7:11815–11823
14. Yun S, Guo T, Zhang J, He L, Li Y, Li H, Zhu X, Gao Y (2017) Facile synthesis of large-sized monolithic methyltrimethoxysilane-based silica aerogel via ambient pressure drying. J Sol-Gel Sci Technol 83:53–63
15. Feng Q, Chen K, Ma D, Lin H, Liu Z, Qin S, Luo Y (2018) Synthesis of high specific surface area silica aerogel from rice husk ash via ambient pressure drying. Colloids Surf Physicochem Eng Aspects 539:399–406
16. Kistler SS (1931) Coherent expanded-aerogels. J Phys Chem 36:52–64
17. Danks A, Hall S, Schnepp Z (2016) The evolution of 'sol–gel' chemistry as a technique for materials synthesis. Mater Horiz 3:91–112
18. He S, Yang H, Chen X (2017) Facile synthesis of highly porous silica aerogel granules and its burning behavior under radiation. J Sol-Gel Sci Technol 82:407–416
19. Estella J, Echeverría JC, Laguna M, Garrido JJ (2008) Effect of supercritical drying conditions in ethanol on the structural and textural properties of silica aerogels. J Porous Mater 15:705–713
20. He F, Zhao H, Qu X, Zhang C, Qiu W (2009) Modified aging process for silica aerogel. J Mater Process Technol 209:1621–1626
21. Smith DM, Stein D, Anderson JM, Ackerman W (1995) Preparation of low-density xerogels at ambient pressure. J Non-Cryst Solids 186:104–112
22. Uchida N, Ishiyama N, Kato Z, Uematsu K (1994) Chemical effects of DCCA to the sol-gel reaction process. J Mater Sci 29:5188–5192
23. Kim CE, Yoon JS, Hwang HJ (2008) Synthesis of nanoporous silica aerogel by ambient pressure drying. J Sol-Gel Sci Technol 49:47
24. Gurav JL, Nadargi DY, Rao AV (2008) Effect of mixed catalysts system on TEOS-based silica aerogels dried at ambient pressure. Appl Surf Sci 255:3019–3027
25. Shi F, Wang L, Liu J (2006) Synthesis and characterization of silica aerogels by a novel fast ambient pressure drying process. Mater Lett 60:3718–3722
26. He S, Huang D, Bi H, Li Z, Yang H, Cheng X (2015) Synthesis and characterization of silica aerogels dried under ambient pressure bed on water glass. J Non-Cryst Solids 410:58–64
27. Smith DM, Maskara A, Boes U (1998) Aerogel-based thermal insulation. J Non-Cryst Solids 225:254–259
28. Liu S, Yao F, Oderinde O, Zhang Z, Fu G (2017) Green synthesis of oriented xanthan gum–graphene oxide hybrid aerogels for water purification. Carbohydr Polym 174:392–399
29. Ebisike K, Okoronkwo AE, Alaneme KK (2019) Adsorption of Cd (II) on chitosan–silica hybrid aerogel from aqueous solution. Environ. Technol Innovation 14:100337

30. Ebisike K, Okoronkwo AE, Alaneme KK (2018) Synthesis and characterization of Chitosan-silica hybrid aerogel using sol-gel method. JKSUS 32:550–554

31. Demilecamps A, Beauger C, Hildenbrand C, Rigacci A, Budtova T (2015) Cellulose–silica aerogels. Carbohydr Polym 122:293–300

32. Nistor MT, Vasile C, Chiriac AP (2015) Hybrid collagen-based hydrogels with embedded montmorillonite nanoparticles. Mater Sci Eng C 53:212–221

33. Jamilah B, Harvinder K (2002) Properties of gelatins from skins of fish-black tilapia (Oreochromis mossambicus) and red tilapia (Oreochromis nilotica). Food Chem 77:81–84

34. Wang B, Bai Z, Jiang H, Prinsen P, Luque R, Zhao S, Xuan J (2019) Selective heavy metal removal and water purification by microfluidically-generated chitosan microspheres: Characteristics, modeling and application. J Hazard Mater 364:192–205

35. Xu C, Shi S, Wang X, Zhou H, Wang L, Zhu L, Zhang G, Xu D (2019) Electrospun SiO2-MgO hybrid fibers for heavy metal removal: characterization and adsorption study of Pb(II) and Cu (II). J Hazard Mater 381:120974

36. Ma H, Wang S, Meng F, Xu X, Huo X (2017) A hydrazone-carboxyl ligand-linked cellulose nanocrystal aerogel with high elasticity and fast oil/water separation. Cellulose 24:797–809

37. Gong JL, Wang XY, Zeng GM, Chen L, Deng JH, Zhang XR, Niu QY (2012) Copper (II) removal by pectin–iron oxide magnetic nanocomposite adsorbent. Chem Eng J 185:100–107

38. Habila MB, Alothman ZA, El-Toni AM, Labis JP, Soylak M (2016) Synthesis and application of $Fe_3O_4@SiO_2@TiO_2$ for photocatalytic decomposition of organic matrix simultaneously with magnetic solid phase extraction of heavy metals prior to ICP-MS analysis. Talanta 154:539–547

39. Mahmoud ME, Fekry NA, El-Latif MMA (2016) Nanocomposites of nanosilica-immobilized-nanopolyaniline and crosslinked nanopolyaniline for removal of heavy metals. Chem Eng J 304:679–691

40. Vergili I, Beril Gönder Z, Kaya Y, Gürdağ G, Cavus S (2017) Lead removal from battery wastewater using synthesized poly (ethyleneglycol dimethacrylatemethacrylic acid) gel bead and poly (methacrylic acid) hydrogel. Polym Bull 74:2605–2624

41. Eid MS, Azzam GH, Eshaq AM, Rabie AA, Bakr AA, Abd-Elaal AE, El Metwally SM (2016) Preparation and characterization of chitosan-clay nanocomposites for the removal of Cu(II) from aqueous solution. Int J Biol Macromol 89:507–517

42. Fang X, Zhu S, Ma J, Wang F, Xu H, Xia M (2020) The facile synthesis of zoledronate functionalized hydroxyapatite amorphous hybrid nanobiomaterial and its excellent removal performance on Pb^{2+} and Cu^{2+}. J Hazard Mater 392:122291

43. Wang H, Wang Z, Yue R, Gao F, Ren R, Wei J, Wang X, Kong Z (2020) Functional group-rich hyperbranched magnetic material for simultaneous efficient removal of heavy metal ions from aqueous solution. J Hazard Mater 384:121288

44. Alsohaimi IH, Wabaidur SM, Kumar M, Khan MA, Alothman ZA, Abdalla Abulhassan M(2015) Synthesis, characterization of PMDA/TMSPEDA hybrid nano-composite and its applications as an adsorbent for the removal of bivalent heavy metals ions Chem Eng J 270:9–21

45. Liu P, Jiang L, Zhu L, Guo J, Wang A (2015) Synthesis of covalently crosslinked attapulgite/poly (acrylic acid-co-acrylamide) nanocomposite hydrogels and their evaluation as adsorbent for heavy metal ions. J Indust Eng Chem 23:188–193

46. Srivastava N, Thakur AK, Shahi VK (2016) Phosphorylated cellulose triacetate–silica composite adsorbent for recovery of heavy metal ion. Carbohydr Polym 136:1315–1322

47. Zhao R, Li X, Sun B, Shen M, Tan X, Ding Y, Jiang Z, Wang C (2015) Preparation of phosphorylated poly acrylo nitrile-based nano fiber mat and its application for heavy metal ion removal. Chem Eng J 268:290–299

48. Anirudhan TS, Ramachandran M (2008) Synthesis and characterization of amidoximated polyacrylonitrile/organobentonite composite for Cu(II), Zn(II), and Cd(II) adsorption from aqueous solutions and industry wastewaters. Ind Eng Chem Res 47:6175–6184

49. Poureteda HR, Kazemi M (2012) Characterization of modified silica aerogel using sodium silicate precursor and its application as adsorbent of Cu^{2+}, Cd2+, and Pb2+ ions. Int J Ind Chem 3:20–28

50. Qin L, Ge Y, Deng B, Li Z (2017) Poly (ethylene imine) anchored lignin composite for heavy metals capturing in water. J Taiwan Inst Chem 71:84–90

51. Huang CH, Hsieh TH, Chiu WY (2014) Evaluation of thermally crosslinkable chitosan-based nano fibrous mats for the removal of metal ions. Carbohydr Polym 116:249–254